International Research Journal of Engineering and Technology (IRJET) e-ISSN: 2395-0056
Volume: 11 Issue: 09 | Sep 2024 www.irjet.net p-ISSN: 2395-0072

# Optimal designing and parameter selection of voltage source inverter for real-time performance analysis in weak grid and standalone mode

**Harendra Pal Singh[1*], Anurag K. Swami[1]**

*[1]Department of Electrical Engineering*
*College of Technology, Pantnagar*
*Uttarakhand, 263145, India*

---

**Abstract -** *This study aims to enhance inverter stability for lower-voltage distribution networks by focusing on grid impedance-based stability. Additionally, it suggests considering IEEE Standard-519 when selecting the ideal filter and controller parameters for weak grids. Two techniques are used to improve inverter stability: (A) altering the grid-side inductance, and (B) changing the VSI's output impedance. The goal is to optimize the VSI controller's and filter design's parameters. To obtain the optimized Current Control Loop (CCL) parameters to maintain the Total Harmonic Distortion (THD) level at the Point of Common Coupling (PCC) and ensure VSI stability during parametric uncertainty, Ziegler-Nichols (ZN), Particle Swarm Optimization (PSO), and a real-coded Genetic Algorithm (GA) are utilized. To validate the effectiveness of the optimized CCL parameters, a real-time simulator, Typhoon HIL, is used to simulate a VSI-based system connected to a weak grid and operating in standalone mode. Various conditions, such as filter inductance variation, grid Short Circuit Ratio (SCR), output power regulation, and sudden load changes in a standalone distribution network, are tested. The VSI-based system's controller model simulation and parameter optimization are performed using MATLAB/SIMULINK with m-files. Regardless of whether the inverter is connected to the grid or not, this paper provides an extensive review of how to select the optimal inverter component parameters and their impact under various real-world conditions*

***Key Words***: Controller stability criterion, Heuristic optimization technique, Power quality, Total Harmonic Distortion, Weak grid condition, Impedance-based stability, Standalone microgrid system.

## 1.INTRODUCTION

Grid Connected Inverters (GCIs) have become a critical component of modern power systems, enabling the integration of various Distributed Energy Resources (DERs) into the main utility grid. These DERs encompass a range of capacities, categorized as lower/small level (less than 10 kW), medium level (10 – 1000 kW), and higher level (1 - 10 MW), each with distinct operational requirements [1]. To ensure the reliable and safe operation of these systems, a set of international and national standards, including those governing operational principles, power quality, safety measures, and responses under abnormal conditions, have been established, offering valuable guidance for application-specific practices, as noted by [2],[3]. Across the globe, widely recognized standards, such as IEEE – 1547 [4], IEC – 61727 [5], IEEE – 929 [6], along with region-specific standards like VDE-AR-4105 (Germany) [7] and RULE-21 (California, USA) [8], play a pivotal role in governing the interconnection of DERs with the grid, ensuring a seamless transition towards cleaner and more sustainable energy systems.

For systems rated at 69 kV and below, IEEE Std. 519 recommends specific limits to ensure the quality of power at the PCC. According to [9], it stipulates that the total harmonic distortion should not exceed 5%, and individual voltage distortion should be within 3%. Additionally, it provides guidelines for limiting the current distortion concerning the short circuit current (Isc) to load current ratio (IL), emphasizing the attenuation of higher-order harmonic components. To gauge the strength of the grid connection, [10] points out that the percentage of current ripples in the inverter output current is a crucial indicator. For weaker grid connections, the standard allows for 0.3% current ripples, while in the case of stronger grid connections, this tolerance can be higher. This approach defines the smoothness of the output current, ensuring compliance with the specified grid connection conditions.
The research work's primary objective is to thoroughly investigate the design of a VSI and its impact on operational performance, particularly under conditions of a weak grid, while simultaneously upholding established power quality standards. In order to attain this goal, it is imperative to gain a comprehensive understanding of how the inverter functions within a distribution network. A weak grid is more susceptible to voltage drops, harmonic distortion, and equipment failures. This is because the higher impedance can cause the voltage to drop more as the current flows through the grid. It can also amplify the effects of harmonic distortion and make it more difficult for equipment to operate reliably. Also, weak grids can undermine sustainability by increasing energy losses, reducing reliability, increasing the cost of electricity, and limiting the integration of renewable energy.

### 1.1 Motivation

The stability of grid-connected inverters can be comprehensively assessed by examining their response to both small and large-scale disturbances within the control signal, as discussed in [11][12]. The small-scale disturbances may not significantly disrupt VSI synchronization with the grid but can manifest their effects during grid feeding, potentially leading to the generation of harmonics and voltage instability at the PCC [13]. To evaluate instability arising from small signals, two distinct methods have been proposed: one based on eigenvalues and the other based on impedance. Furthermore, in such operating conditions, the interplay between the Phase Locked Loop (PLL) and CCL can introduce current distortion, emerging as a key factor in potential system instability, as outlined by [11]. Effective damping mechanisms play a pivotal role in preserving system equilibrium during transient network conditions. This research, therefore, conducts a comprehensive exploration of inverter stability issues, particularly when operating in weak grid scenarios and amidst dynamic conditions.

Traditionally, impedance-based system stability criteria have solely relied on network impedance, regardless of variations in the current reference [14]. In reality, the current reference can also affect the stability of a power system. For example, if the current is measured at a point on the grid where the impedance is high, then the system is more likely to become unstable. Therefore, the impedance-based stability approaches have been outlined, including (a) designing control strategies that enhance adaptability to changes in grid impedance, (b) adjusting the output impedance of the VSI when it's connected in parallel with other devices or passive components, and (c) considering impedance variations in filter design and VSI control, where parameters are determined based on grid-side impedance changes to prevent instability conditions [15], [16]. However, it's important to note that in weak grid conditions, the grid impedance can interact with the CCL, potentially leading to system instability. This paper explores all three of these methods in experimental scenarios.

Microgrid management strategies are designed to attain optimal power scheduling through the implementation of controller actions. Two distinct approaches have been put forth: the Rule/Reference-based approach and the Predictive optimization-based approach. The Tunable- Rule/Reference-Based-Heuristic (TRBH) approach offers a notable advantage by inherently furnishing a re-setting strategy. This is achieved by computing a specific outcome based on a particular illustration conforming to the optimal tuning dispatch rule. Consequently, predictive optimization is not recommended as the primary controlling method [17].

### 1.2 Literature Review

In grid-connected mode, the grid is the dominant factor, and it is generally assumed that the operation is stable under these circumstances. This means that when a microgrid is connected to the main grid, the main grid is the primary source of power and control, and it is typically expected to be in a stable and reliable state. However, when confronted with weak grid scenarios, the primary focus shifts toward evaluating the controller's performance and its adaptability to impedance variations. For lower and medium-level VSIs, improvements in the inverter switch control, combined with well-designed filters, have proven advantageous in enhancing the quality of the output current, discussed in [18] and [19]. Nevertheless, these enhancements may impact the control bandwidth and the variation in grid-side impedance. To achieve better performance and power supply quality, it is imperative for the current control loop to exhibit higher control band- width and swift dynamic response. Prior studies [20],[21], underscore the importance of judiciously selecting controller gain values based on filter design and power-sharing criteria, necessitating precise specification of the control range. Controller parameters must be meticulously designed to minimize errors resulting from anticipated input values. However, the core concept of current regulation entails comparing reference and measured output current values, enabling error utilization to modulate power electronic converters' switching for the attainment of desired output [22].

Throughout history, various methods have emerged to efficiently tune PID/PI controllers, particularly for systems with complex, inverse responses. These methods, like Ziegler-Nichols (1942) [23], Cohen-Coon (1953), and Tyreus-Luyben (1997), rely on inherent process characteristics and involve oscillatory approaches. While established, these methods are known for being time-consuming and imprecise due to their reliance on trial-and-error. In contrast, the Internal Model Control (IMC) method, introduced by Rivera (1986) [24], utilizes a fitness function to determine optimal controller parameters directly, offering a more efficient and accurate solution.

Within the realm of computational intelligence algorithms, including Artificial Neural Networks (ANN), Genetic Algorithms (GA), Particle Swarm Optimization (PSO), Predictive Model Control (MPC), and others, these techniques offer promising solutions for accurately determining controller gain values [25],[26]. PSO, in particular, has gained widespread acceptance owing to its simplicity, computational efficiency, and robustness, as it was originally introduced by Kennedy and Eberhart in 1995 [27], [28]. Over time, through a trial-and-error procedure, various algorithm parameters have been refined for ease of implementation across diverse applications, as seen in Eberhart, Simpson, and Dobbins (1996). The PSO algorithm can accommodate different fitness functions tailored to specific objectives. For instance, the Integral of Time multiplied by Absolute Error (ITAE) performance index criteria for control system design was introduced by Graham

**Table -1:** COMPARISON OF REAL CODED GA AND PSO

| *Factors* | *Real-coded GA* | *PSO* |
|---|---|---|
| **Representation** | Chromosomes (strings of genes) | Particles (position and velocity) |
| **Search mechanism** | Particles (position and velocity) | Velocity and position updates based on individual and social learning |
| **Strengths** | Global search, good at finding diverse solutions | Fast convergence, efficient for problems with continuous decision variables |
| **Weaknesses** | Can be slow to converge, prone to getting stuck in local optima | Can be sensitive to parameter settings |
| **Robustness to noise** | More robustness to noise than PSO | Less robust to noise than GA |
| **Data types** | Can be binary, integer, or real | Can be binary, integer, or real |
| **Ability to solve multi-objective problems** | Can solve multi-objective problems | Typically only used to solve single-objective problems |

and Lathrop in 1953 [29]. The PSO algorithm's implementation shares similarities with Genetic Algorithms (GA), initializing with a population of random solutions [30]. Table 1 compares real-coded GA and PSO, and shows that real-coded GA are better suited for implementation in this case, especially in terms of representation and robustness to noise. Also, real coded based GA is a better suited for the problems with real variables. To ensure closed-loop performance and system stability, the Routh-Hurwitz (R-H) criteria can be employed to define the boundaries of the search space based on the closed-loop characteristic equation [31]. Advanced Digital Signal Processors (DSPs) play a vital role in reducing control delay time and enhancing system responsiveness, thus bolstering overall system reliability. Additionally, Field Programmable Gate Array (FPGA) circuits and the Space Vector Pulse Width Modulation (SVPWM) technique prove valuable for addressing issues like signal delay, dead-time, and mitigating output current harmonics [32].

Ensuring the stability and reliability of a distribution network requires the design of a robust VSI, with careful consideration of critical factors like grid impedance variations and the maintenance of power quality. However, in situations where generation systems are situated in remote areas, the medium-voltage transmission lines may be extended, resulting in a significant inductive grid impedance [33]. High grid impedance characterizes what is commonly referred to as a weak grid. In accordance with IEEE Std. 1204-1997 [34], a grid is typically deemed weak when the Short Circuit Ratio (SCR) is less than three. Weak grids are often encountered in remote or rural areas that rely on lengthy feeder lines for their power supply.

Based on the preceding discussions, we have prepared a comprehensive comparison, as presented in Table 2. This table is instrumental in highlighting the unique contributions of this paper by contrasting it with various prior works from the literature. It not only aids in gaining a fundamental comprehension of VSI component design and parameter selection but also provides practical insights for real-world validation.

### 1.3. Contribution

A comprehensive discussion on VSI design and parameter selection for the lower voltage network level is presented here. The primary focus revolves around addressing two key challenges: managing impedance variations at the PCC and enhancing the tracking performance of the CCL. Regarding this, the paper shows the validation and main contributions of this work as follows:

**(i).** The paper's primary contribution is an improved controller for VSIs, enhancing dynamic response in low voltage networks, especially during transients. It emphasizes the need for controller stability to prevent instability in weak grid conditions. The paper also introduces a method to select VSI filter parameters, aiming to minimize stored energy in components while improving THD levels at the PCC.

**(ii).** The paper examines the robustness of the proposed single loop controller in regulating the VSI's behavior under diverse operational conditions.

**(iii).** Through simulations on a real-time simulator, Typhoon HIL, the study validates the effectiveness of optimized CCL parameters. These parameters are assessed under varying conditions such as changes in grid-side inductance, grid SCR, and abrupt load changes, both in a VSI-based system connected to a weak grid and in a standalone distributed network. This analysis serves to confirm the controller's

tracking performance in real-time scenarios, ensuring its reliability and adaptability across different conditions.

**(iv).** The two methods are employed to enhance inverter stability: (a) changing the output impedance of the VSI by adjusting the grid-side inductance, and (b) optimizing the parameters for filter design and VSI controller.

The paper additionally introduces the implementation of a Proportional-Resonant (PR) con- troller in the proposed VSI approach. This addition aims to enhance harmonic attenuation at the PCC, particularly in the presence of weak grid conditions, with the ultimate goal of improving the THD level.

The paper presents a comprehensive analysis of plant model-based tuning rules and outlines various factors to consider for optimizing the current controller gain values of VSI to address varying production rates and different grid scenarios. This flexibility enables the controller to be fine-tuned to specific operating conditions, thereby enhancing its overall performance and adaptability in practical scenarios. This paper is described in the following sections: *Section 2* details the system description, *Section 3* describes filter designing and parameters selection, *Section 4* elaborates controller modeling; PSO algorithm and real coded based GA implementation, and sensitivity/fitness function, *Section 5* gives results and discussion of the different scenario analysis, and *Section 6* concludes the work done in the paper.

**TABLE – 2:**
COMPARATIVE ANALYSIS ACROSS VARIOUS REFERENCE SOURCES IN THE LITERATURE.

| Items | References | This paper |
|---|---|---|
| Standards and regulations | [1],[2],[3],[4],[9],[10][34] | ✓ |
| Different modeling methods | [18],[20],[35] | SRF and SF |
| Filter designing | [10],[36],[37],[38],[39] | with minimum energy storage |
| Different control techniques | [21],[22],[17],[40].[41] | VOC with PI and PR controllers |
| Controller tuning techniques | [23],[24] | ZN, PSO and GA implementation |
| Optimization techniques | [25],[26],[27], [28],[29],[30] | heuristic approach |
| Stability analysis | [31],[12],[42] | in grid following and forming modes |
| Impedance based stability | [33],[11],[13],[14],[16], | ✓ |
| Real-world implementation | [32],[12], | with consideration of different conditions |

## 2. SYSTEM DESCRIPTION

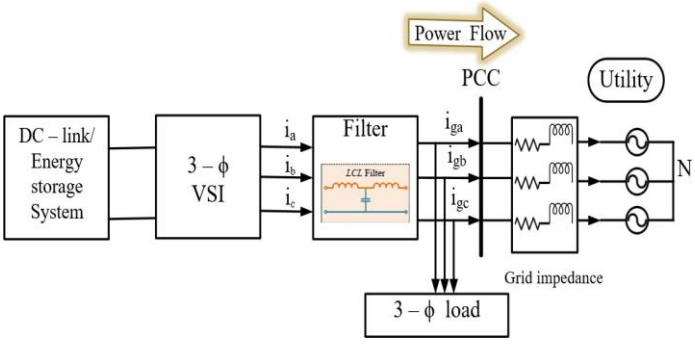


**Fig -1**: VSI System in GFL mode

In a grid-feeding mode, a VSI-based system functions as a controlled current source, as shown in Fig. 1, and plays a vital role in meeting power supply and demand requirements [18],[20]. Moreover, the grid-feeding (GFL) VSI-based system injects output current while closely tracking the PCC voltage. It also offers higher impedance to grid disturbances and noise, contributing to the overall enhancement of power quality within the system. Voltage-oriented control is the common choice in VSI-based systems for synchronization and control purposes [40]. Notably, power to the grid can be effectively regulated by controlling the output current of the VSI-based system, especially when the grid voltage remains relatively constant. Fig. 2 illustrates a grid-connected VSI with an LCL filter, taking 3-ϕ output voltage and current as inputs for the controllers. The switching signals for the VSI are generated using the SVPWM scheme.

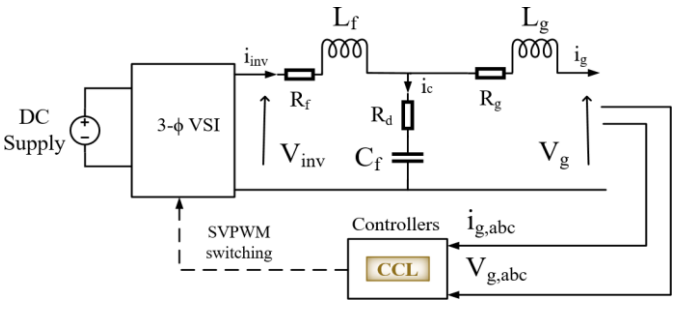


**Fig -2**: Schematic diagram of grid connected VSI with LCL filter

The objective of the controller is to adequately control the output current of the VSI by following the active power command given by the operator. As the controller follows the grid voltage and injects the current to the PCC, hence, power quality issues present in the PCC voltage worsen the power

quality of the output current of the VSI. However, the output current's power quality can also be improved by appropriately designing the filter components and the control parameters. Here, the designing purpose parameters associated with the VSI are to improve the system efficiency in terms of reliability, resiliency, and redundancy and the power delivered to the utility with improving the power quality. The inverter output voltage and current from Fig. 2 can be written as,

$$\begin{bmatrix} V_{inv,a} \\ V_{inv,b} \\ V_{inv,c} \end{bmatrix} = R \begin{bmatrix} i_{g,a} \\ i_{g,b} \\ i_{g,c} \end{bmatrix} + \omega L_T \begin{bmatrix} \frac{di_a}{dt} \\ \frac{di_b}{dt} \\ \frac{di_c}{dt} \end{bmatrix} + \begin{bmatrix} V_{g,a} \\ V_{g,b} \\ V_{g,c} \end{bmatrix} \quad \textbf{(1a)}$$

$$i_{inv,abc} = i_{c,abc} + i_{g,abc} \quad \textbf{(1b)}$$

where $V_{inv\{.\}}$ , $i_{inv\{.\}}$ , $i_{g\{.\}}$ , $i_{\{.\}}$ , $i_{c\{.\}}$ and $V_{g\{.\}}$ represents inverter output voltage, inverter output current, grid feeding current, inductor current, capacitor current and the grid voltage of $\{a, b, c\}$ phase respectively. The $R = (R_f + R_g)$, and $L_T = (L_f + L_g)$ where $R_f$, $R_g$, $L_f$ and $L_g$ are the inverter side and grid side filter resistance and inductance respectively. $R_d$ is a damping resistor. The $C_f$ is the filter capacitance and $\omega$ is the grid frequency.

## 3. FILTER DESIGNING AND PARAMETERS SELECTION

The filter acts as an intermediary between the VSI and PCC, enhancing the quality of the out- put current in compliance with *IEEE Std.519* guidelines. *IEEE Std.519-2022* [43], also concerned for harmonic control in electric power systems, which was updated from *IEEE Std.519-2014* [44] to include more stringent harmonic limits at the PCC between the utility and the customer. This is necessary to accommodate the increasing number of non-linear loads on the power system, such as variable frequency drives, and switch-mode power supplies. In grid-connected mode, the proper selection of the filter and power-sharing parameters ensures the power quality within the regulated range and enhances the system performance against the transient conditions. The percentage of current ripple limits and harmonic distortions in output current recommendations are given in Table 3, which helps to design the filter components for the VSI-based system.

The higher switching frequency operation inverter applications avoid the use of only inductive components in the filter for the medium and higher power rating inverters because of the bigger size requirement which turns into costly and higher voltage drop across it [36]. Compared to first and second-order filters, the third-order LCL filter has a lower cost and is smaller in size which makes it more suitable for the inverter output connection with the main utility at medium and higher voltage levels. LCL filter provides excellent attenuation of bode 60 dB to the switching frequency Fig. 3. But, in case the grid side impedance is lower, resonance can be triggered, leading to system instability [10]. Moreover, this resonance effect can subsequently cause voltage and current instability in proximity to the resonance frequency. The purpose of applying the resistive damper is to reduce the attenuation and increase the damping (*Q - factor*) at the characteristic resonance frequency with the minimum power loss.

**TABLE-3**: CURRENT HARMONIC LIMITS IN THE PERCENTAGE OF RATED CURRENT AMPLITUDE ACCORDING TO IEEE 519.

| | Maximum odd harmonic current distortion in percent of $I_L$ for general distribution system (120 V - 69 kV) | | | | | |
|---|---|---|---|---|---|---|
| $\frac{I_{sc}}{I_L}$ | $h < 11$ | $11 \le h < 17$ | $17 \le h < 23$ | $23 \le h < 35$ | $35 \le h$ | TDD |
| < 20 | 4.0 | 2.0 | 1.5 | 0.6 | 0.3 | 5.0 |

*$h$ is the order of harmonics, TDD is Total Demand Distortion

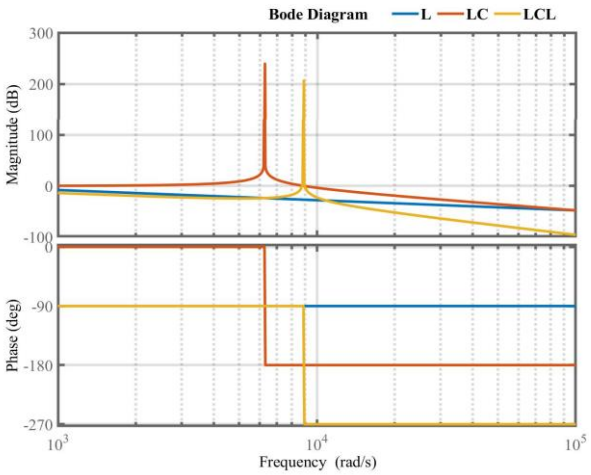


**Fig - 3:** L, LC and LCL filter bode plot.

In summary, the design of the LCL filter concerns the following points;

- Overall filter size, cost, losses
- Current distortion in different components
- Resonance and dynamic performance of the overall system
- Low voltage drops across the filter
- Higher power factor.

The parameter selection, according to the recommended maximum current distortion limit in the output current set the percentage of current ripples in the inverter output current is the primary concern to describe the lower limit of the filter inductance value. Similarly, the filter capacitance is chosen based on the energy stored in the capacitor. The selection for the filter capacitor is a trade-off between the energy stored in the capacitor and the inverter-side inductance ($L_f$)[39]. The higher value capacitance uses more reactive power to flow into the capacitor and more load current demand from the $L_f$ and the inverter switches. As a consequence, the system efficiency will be decreased. The

filter inductive reactance should be lower than the capacitive reactance, so the lower the voltage drop across $L_f$. Generally, the reactive power for the capacitor is chosen between 5 - 15% of the rated capacity as per the requirement.

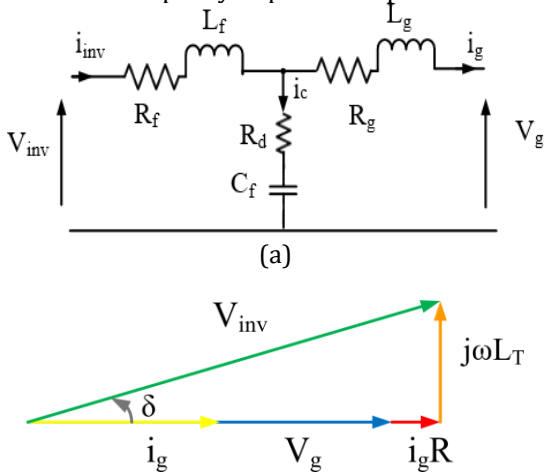


**Fig - 3:** (a).Equivalent circuit diagram of LCL filter connected between VSI and grid, (b). Phasor diagram for the unity power condition.

The following equations represent the circuit shown in Figure 4 (a) and (b). These equations will be employed to compute the transfer function of the LCL filter:

$$V_{inv} = S\frac{V_{dc}}{2} \quad \textbf{(2a)}$$

$$i_c = i_{inv} - i_g \quad \textbf{(2b)}$$

$$V_{inv} = i_{inv}(R_f + sL_f) + i_c\left(\frac{1}{sC_f} + R_d\right) \quad \textbf{(2c)}$$

$$V_g = -i_g(R_g + sL_g) + i_c\left(\frac{1}{sC_f} + R_d\right) \quad \textbf{(2d)}$$

where, $V_{inv}$ is the inverter output 3 – $\phi$ voltage vector, $S$ represents the switching space vector, $V_{dc}$ is the DC - link voltage, $i_c$ is the capacitor current, $i_{inv}$ and $i_g$ are the inverter-side and grid-side currents.

The transfer function of the LCL filter network $G_p(s)$ is considered as a plant for the controllers and calculated from the ratio of output grid current $i_g(s)$ to the inverter output voltage $V_{inv.}(s)$ is represented in (3);

$$G_p(s) = \frac{i_g(s)}{V_{inv}(s)} = \frac{a_1 s + 1}{b_3 s^3 + b_2 s^2 + b_1 s + b_0} \quad \textbf{(3)}$$

where, $a_1 = R_d C_f$, $b_3 = L_f L_g C_f$, $b_2 = C[(L_f + L_g)R_d + L_g R_f + L_f R_g]$, $b_1 = R_d R_g C_f + R_d R_f C_f + R_f R_g C_f + L_f + L_g$, $b_0 = R_f + R_g$. Here, $b_3$, $b_2$, $b_1$ are the grid-side inductance dependent coefficients, which affect the grid connection (stiff/weak grid) requirements.

The resonance frequency of LCL filter is calculated by using (4);

$$f_{res} = \frac{1}{2\pi}\sqrt{\frac{L_T}{L_f L_g C_f}} \quad (4)$$

Generally, the initial operating conditions of VSI should be determined before selecting the filter parameters, like rated power ($P_{rated}$), rated $i_{inv}$, output voltage $V_{inv}$, inverter switching frequency, $f_{sw}$, fundamental frequency, $f_0$. The steps for choosing the LCL filter parameters are as follows:

***Step 1.*** Determine the maximum value for the inverter-side inductance, $L_f$, based on the maximum value of current ripples in the output current as follows:

$$L_{f(max)} = \frac{V_{dc} D}{4 f_{sw} \Delta i|_{max}} \quad (5)$$

where $V_{dc}$ is the input DC voltage, that can obtain from $(2\sqrt{3}V_{(g,rms)}/M)$ here M is the modulation index, D is the duty cycle, $\Delta i|_{max}$ is maximum current ripple, that is generally set to be 20 - 30%. As given in [10], to calculate the minimum inductance value based on switching frequency is given as;

$$L_{f(min)} = \frac{1}{|\omega_{sw} * \left(\frac{i_{g(sw)}}{V_{i(sw)}}\right) * \left(1 - \left(\frac{\omega_{sw}}{\omega_{res}}\right)^2\right)|} \quad (6)$$

***Step 2.*** As discussed earlier, determine the filter capacitor value based on the maximum reactive power stored in the capacitor as given below;

$$C_f = 15\% \frac{P_{rated}}{3\omega_0 V_g^2} \quad (7)$$

where $P_{rated}$ is the VSI power rating, $\omega_0$ is fundamental angular frequency.

***Step 3.*** Based on selection of switching frequency, $f_{sw}$, determine the filter cut-off frequency as $(1/10^{th})$ of $(f_{sw})$.

***Step 4.*** Determine the minimum inductance value at selected $f_{sw}$ according to the IEEE std. as defined in table II current distortion and harmonic limits, as given in (6).

***Step 5.*** The maximum and minimum value of inductance provides a selection range for the inverter-side and grid-side inductors to choose the suitable values based on harmonic attenuation and the inductance ratio $a_L$ (i.e., $a_L = L_f/L_g$). The resonance frequency decreases as the grid-side inductance increases with respect to the inverter side. The ratio $a_L = 1$, i.e., $L_f = L_g$, corresponds to the minimum capacitance requirement and lower harmonic attenuation [10].

***Step 6.*** The THD level of the output current must be below 5%. If THD is higher than 5% then decrease the attenuation rate and design the new filter parameters.

Generally, the filter parameters selection includes filtering and controlling issues, which is a trade-off between better filter action (minimum current distortion) and fast dynamic performance. Selected filter parameters are given in the Table 5. The trade-off is shown in the result, Section 5.1.1, and minimum current distortion, means better tracking of the reference value.

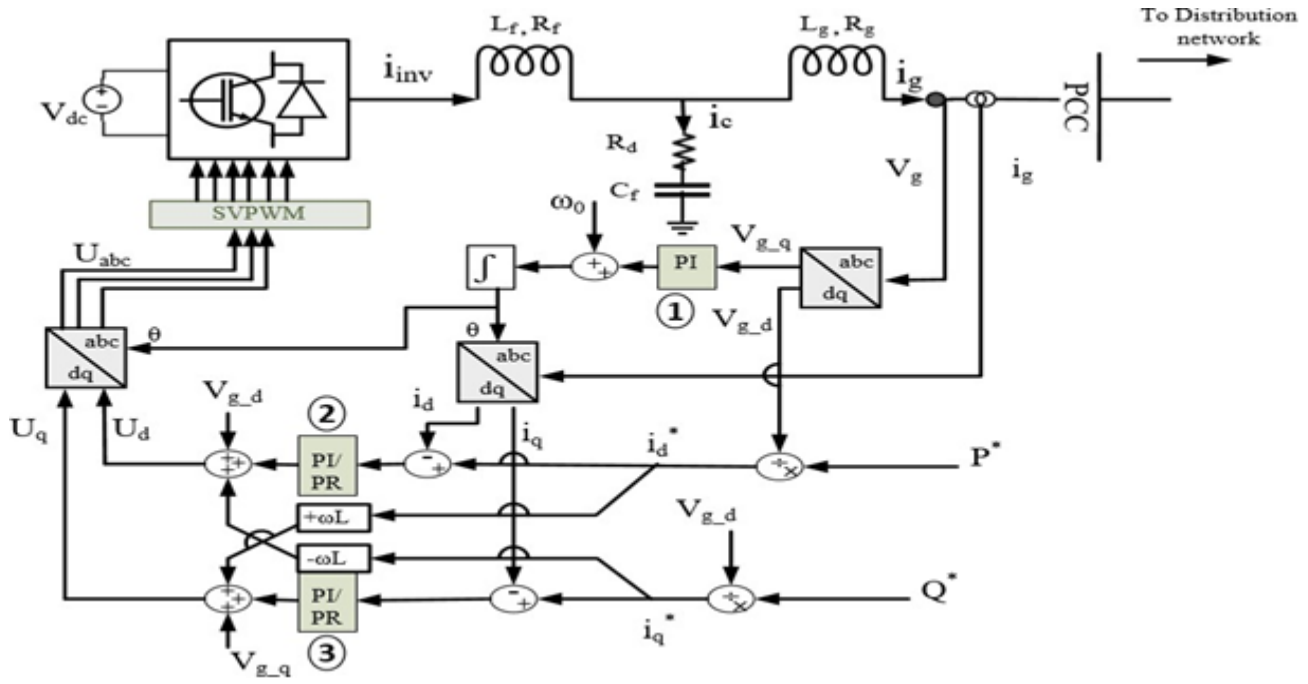


**Fig - 5:** 3ϕ SRF Controller for VSI in GFL mode

## 4. CONTROLLER MODELLING

In situations where a weak grid connection exists, there is a risk that the controllers may struggle to accurately follow the grid's voltage or angle as a reference, potentially leading to instability in the system. To mitigate this, it's essential to configure the gain values within the CCL according to the characteristics of the plant model to ensure precise tracking performance. Consequently, in order to optimize the performance of Local Control Units (LCUs), it is imperative to meticulously design and fine-tune the control parameters.

This is especially critical for maintaining system stability across a wide spectrum of operating conditions, particularly in low voltage distributed networks [12].

The adaptive control scheme is built upon a cascaded feed-forward control structure, featuring two control loops, the inner and outer loops, operating in the Synchronously Rotating Frame (SRF) and the Stationary Frame (SF). In this context, the primary focus of controller modeling is on the inner loop, which is meticulously designed to minimize settling times during power regulation and to enhance system dynamic performance. It is important to highlight that a single-loop control scheme while offering a compromise between fast control dynamics and stable steady-state performance, is typically less robust due to its sensitivity to grid noise (such as harmonics, voltage sags, or transients) [41]. However, it's essential to acknowledge the interdependence between active and reactive powers, and the existence of filters and source inductance can lead to the occurrence of a non-unity power factor current. This, in turn, introduces a cross-coupling term linking the d-axis and q-axis within the SRF, which can have a detrimental effect on controller performance and power regulation.

In the context of GCI systems, employing decoupling techniques is essential for mitigating sensitivity to load changes, enhancing disturbance rejection capabilities, and reducing the output current THD, particularly when dealing with non-linear loads. It's evident that the controller plays a pivotal role in shaping the quality of the current supplied to the primary utility, ensuring a sinusoidal output with minimal THD.

The most widely used PI and PR controllers are considered controllers for the inverter output current regulation. The relationship given for the system in equation 1(a), is converted into the synchronous frame as;

$$V_{i-d} = Ri_d + \omega L_T \frac{di_d}{dt} + V_{g-d} - \omega L_T i_q \quad \textbf{(8a)}$$

$$V_{i-q} = Ri_q + \omega L_T \frac{di_q}{dt} + V_{g-q} + \omega L_T i_d \quad \textbf{(8b)}$$

From the above equations, the active and reactive powers can be calculated as:

$$P_i = 1.5(V_d i_d + V_q i_q) \quad \textbf{(9a)}$$

$$Q_i = 1.5(V_q i_d - V_d i_q) \quad \textbf{(9b)}$$

The current injected into the grid is expected to be in phase with grid voltage which makes the operation at unity power factor. Therefore, $V_q = 0$, in eq. (9a) and (9b), we get; $P_i = 1.5\ V_d i_d$ and $Q_i = -1.5 V_d i_q$, which provides decoupling for the better controlling between the active and reactive power flow to the grid.

### 4.1 Current Controller Structure

The adaptive current control scheme is deliberately designed with relatively lower complexity to accommodate the challenges posed by varying system parameters. In this

approach, the grid-side voltage ($V_g$) and current ($i_g$) variables serve as key input parameters for the CCL. The direct axis current ($i_d$) component is computed using the measured output current, and the necessary phase angle for this conversion is generated by the PLL. The id component is then compared with the reference value $i_d^*$ to generate modulating voltage signals as per equations (10a), (10b).

From Fig. 5, the operation of the current controller in SRF can be expressed as :

$$U_d = \left(K_p + \frac{K_I}{s}\right)(i_d^* - i_d) - \omega L_T i_q + V_{g-d} \quad \textbf{(10a)}$$

$$U_q = \left(K_p + \frac{K_I}{s}\right)(i_q^* - i_q) + \omega L_T i_d + V_{g-q} \quad \textbf{(10b)}$$

where $K_P$ is the proportional and $K_I$ is the integral gain values of the PI controller.

The PI controller in *dq* frame exhibits a single pole at zero frequency, resulting in infinite gain. However, it is incapable of eliminating steady-state error at the fundamental frequency. In a positive sequence SRF, the PI controller behavior is equivalent to the PR controller in SF [21]. Alternatively, the PR controller in $\alpha\beta$ frame is advantageous due to its high gain at the resonant frequency. As per the IMC principle, it can eliminate the steady state error while tracking the sinusoidal signal and provides better harmonic attenuation. The additional damping factor in the ideal resonant term makes the PR controller more reliable for practical applications and can be represented as expressed in (11);

$$G_{PR} = K_P + K_I \frac{s}{s^2 + 2\xi\omega_c s + \omega_0^2} \quad \textbf{(11)}$$

where $\omega_0$ is system fundamental angular frequency, $\omega_c$ is cut-off frequency, $\xi$ is damping factor.

To maintain the robustness of the PR controller, the $\omega_c$ bandwidth must be close enough to the system frequency. If the system frequency varies significantly, the $\omega_c$ can be adjusted accordingly. Therefore, in comparison to PI controller, the PR controller has an advantage in closed-loop performance for frequency variations.

As depicted in Fig. 5, it's evident that the reference voltage and current are derived from the PCC. These reference signals can be distorted due to the weak grid conditions. This distortion has an impact on the CCL performance, which needs to be enhanced to improve the overall performance of the VSI. When using a single-loop control system in the presence of grid noise, such as fluctuations or disturbances in the electrical grid, the stability of the VSI is compromised. Grid noise may introduce unpredictable variations in the electrical parameters that the control system relies on, leading to instability in the VSI's operation. As a result, the effectiveness of the single-loop control system in regulating the VSI's behavior is limited or constrained. Determining the appropriate controller gain values is critical in control system design. It ensures the system stability while achieving the desired level of tracking performance and meeting the safety and performance requirements. The controller tuning purpose is to minimize the overshoot and time response for transient conditions. When the parametric uncertainty and performance specifications are fixed, controller parameters can be optimized for any possible case.

***Problem Formulation***

To enhance the stability of a VSI, the controller gain values, filter parameters, and power- sharing parameters must be kept within the prescribed limits. The optimization of controller parameters is synthesized with the offline procedure, ensuring the operating range of the other components. The performance index is based on error (e) minimization and used for further optimization implementation as given in the following equation;

$$min \int_0^\infty |e(t)|\, dt \quad \textbf{(12)}$$

**s.t.,** $K_{P\,max} > K_P > K_{P\,min}$ , $K_{I\,max} > K_I > K_{I\,min}$

Where, $K_{P\,max}$ and $K_{P\,min}$ are the maximum and minimum values of the proportional gain and $K_{I\,max}$ and $K_{I\,min}$ are the maximum and minimum values of the integral gain of the PI controller.

## 4.2 Fitness Function

The ITAE performance index criteria to design a control system is derived by using a set of $2^{nd}$- order to $8^{th}$-order normalized transfer function coefficients to minimize the ITAE index criteria for a step signal [29]. Since it can provide high disturbance rejection capability to the controllers and minimize the overshoot during transients. This index is also often used for small data sets or data obtained from the step response. ITAE performance index trades-off between error magnitude and settling time [45]. In this paper, the fitness function for the controller tuning is based on minimizing the ITAE, which is calculated by using Simpson's 1/3 rule. The expression for the ITAE performance index is given by (13);

$$ITAE = \int_0^\infty t\, |e(t)|\, dt \quad \textbf{(13)}$$

where, $t$ is the time and $e(t)$ is the error produced by the difference between reference and measured value.

## 4.3 PSO Implementation

PSO is an iterative method that depends on the problem searching space to determine the optimal solution for the fitness function shown in Fig. 6. This algorithm is evaluated based on the movement of each particle and the swarm experience. Each particle movement is based on its own experience and collaboration of the swarm. It attracts towards the best local position ($X_{(p,best)}$) experienced by its own and best global position ($X_{(g,best)}$) by the swarm. The basic rules of the PSO algorithm can be briefly described in the following stages; (a). Finding out the fitness value of each

particle, (b). Updating the best local and global positions, (c). Updating velocity and best global position.

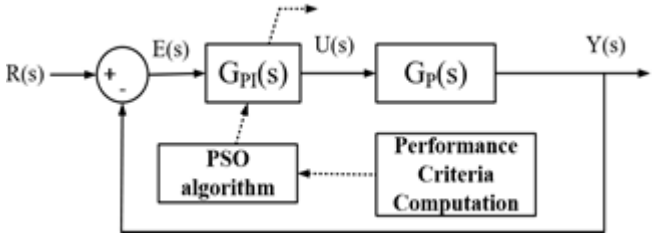


**Fig – 6:** Block diagram of controller tuning using PSO algorithm.

Mathematically, the search process can be represented by the simple equations with concerning position vector $X_i = (x_{i1}, x_{i2}, \ldots, x_{in})$ and velocity vector $V_i = (v_{i1}, v_{i2}, \ldots, v_{in})$ within the specified selection range. The optimality of the solution depends on each particle's velocity and position which is updated as equation 14 in the algorithm.

$$V_i^{k+1} = \omega . V_i^k + c_1 . r_1 \left[X_{p,best}^k - X_i^k\right] + c_2 . r_2 \left[X_{g,best}^k - X_i^k\right] \quad \textbf{(14a)}$$

$$X_i^{k+1} = X_i^k + V_i^{k+1} \quad \textbf{(14b)}$$

where, $i$ represents the index of the particle; $X_i^k$ and $V_i^k$ defined as the position and velocity of the particle $i$ at $k^{th}$ iteration, respectively; $w$ represents the inertia weight which can set between [0-1] (a small inertia weight helps in explore the search space while a large inertia weight facilitates in exploit the search space), and also provides the balance between local and global explorations and exploitations which results in fewer iterations on average to find a sufficiently optimal solution; $c_1$ and $c_2$ are the acceleration constants used to guide the particle's movement to the $p_{best}$ and $g_{best}$ positions; $r_1$ and $r_2$ are the random number variable between [0-1].

Bounded searching space provides fast solutions, but in case the optimum global value is located outside of the boundary conditions, it influences the optimality of the solution [25]. However, the boundary conditions can be extended but this would increase the calculation time and can affect the optimal solution. Therefore, sufficient information about the system parameters limit is beneficial to set the boundary conditions for the search.

### 4.4 GA Implementation

The implementation of GA is the same as the PSO algorithm and a search mechanism to find out the optimal solution from the given problems, which is inherently based on its natural selection. GA provides a solution based on the chromosomes that can adapt to the change in the surrounding environmental conditions and are able to reproduce crossover and mutation. In other words, GA simulation is based on the "survival of the fittest" among individual steps of consecutive generations for solving a problem. So, the solution for each successive generation is more adaptable for their search space. The simulated binary crossover (SBX) operator uses a parameter (known as distribution index, $\eta_c$) to maintain the positive integer value during the overall running time of the simulation. This parameter has a direct effect on controlling of generation of offspring solutions [46]. The generation of offspring $x_i^{(1,t+1)}$ and $x_i^{(2,t+1)}$ from the parent $x_i^{(1,t)}$ and $x_i^{(2,t)}$ is defined as;

$$\beta_i = \left| \frac{x_i^{(1,t+1)} - x_i^{(2,t+1)}}{x_i^{(1,t)} - x_i^{(2,t)}} \right| \quad \textbf{(15)}$$

where, $\beta_i$ is called as the spread factor. The probability distribution index ($\eta_c$) plays a crucial role in single-point crossover (SPX) by influencing the "search power" of the offspring solution. The probability distribution index allows to control the "spread", which affects the diversity of offspring solutions around the parents. Higher values of $\eta_c$ (closer to 20) lead to offspring with values closer to the parent's average, limiting exploration. Lower values of $\eta_c$ (closer to 2) generate offspring with values further away from the average, encouraging exploration. The probability distribution index is used to create an offspring with similar search power in single point crossover, which can be represented as in (16);

$$P(\beta_i) = \begin{cases} 0.5(\eta_c + 1)\beta_i^{\eta_c} & , \quad if \ \beta_i \le 1 \\ 0.5(\eta_c + 1)\dfrac{1}{\beta_i^{\eta_c+2}} & , \quad otherwise \end{cases} \quad \textbf{(16)}$$

By using the random number and the probability distribution function, helps to select a new value "$\boldsymbol{\beta_{qi}}$" for a specific characteristic of the offspring in the evolutionary algorithm. This value is chosen in a way that reflects the desired distribution of characteristics in the population, guiding the algorithm towards promising solutions. From a defined probability distribution index, the ordinate "$\boldsymbol{\beta_{qi}}$" is found which is helpful for the offspring generation as given in the following eqns.;

$$x_i^{(1,t+1)} = 0.5\left[(1 + \beta_{qi})x_i^{(1,t)} + (1 - \beta_{qi})x_i^{(2,t)}\right] \quad \textbf{(17a)}$$

$$x_i^{(2,t+1)} = 0.5\left[(1 - \beta_{qi})x_i^{(1,t)} + (1 + \beta_{qi})x_i^{(2,t)}\right] \quad \textbf{(17b)}$$

Crossover is performed with a higher probability ($P_c$), whereas the mutation is performed with a low probability ($P_m$), see Table 5. If the mutation probability is kept very low, then no element would be mutated by the mutation operator.

Generally, when the fitness function is provided to GA, it is used to observe the behavior of the function in the given criterion of the problem. So, in the case of the minimization of objective function value, the lowest value would be the most suitable solution for the given situation. The developed algorithm is proposed to find out the optimal controller gain values based on the minimum error.

The finally designed VSI components' parameters are tested under dynamic operating conditions in standalone mode for stability analysis. In standalone mode, three VSI sources are considered to create an isolated microgrid environment with critical and non-critical loads, as shown in Fig. 7. The main purpose of this standalone network system

is to evaluate the stability and performance of the designed VSI in terms of frequency and voltage stability during the transient condition. It is crucial to investigate any potential disturbance in microgrids, particularly in the islanded mode, because the inertia is low. When operating in the droop control mode, the bus frequency and voltage amplitude reflect, respectively, the output active and reactive power that satisfies the *P-f* and *Q-V* droop characteristics. The droop characteristic equations can be expressed as;

$$f = f^{ref} - m(P - P^{ref}) \quad \textbf{(18a)}$$

$$V = V^{ref} - n(Q - Q^{ref}) \quad \textbf{(18b)}$$

where, m and n are the droop coefficients, $f^{ref}$ and $V^{ref}$ are the bus frequency and voltage amplitude at the PCC and $P^{ref}$ and $Q^{ref}$ are the active and reactive power of the DG units.

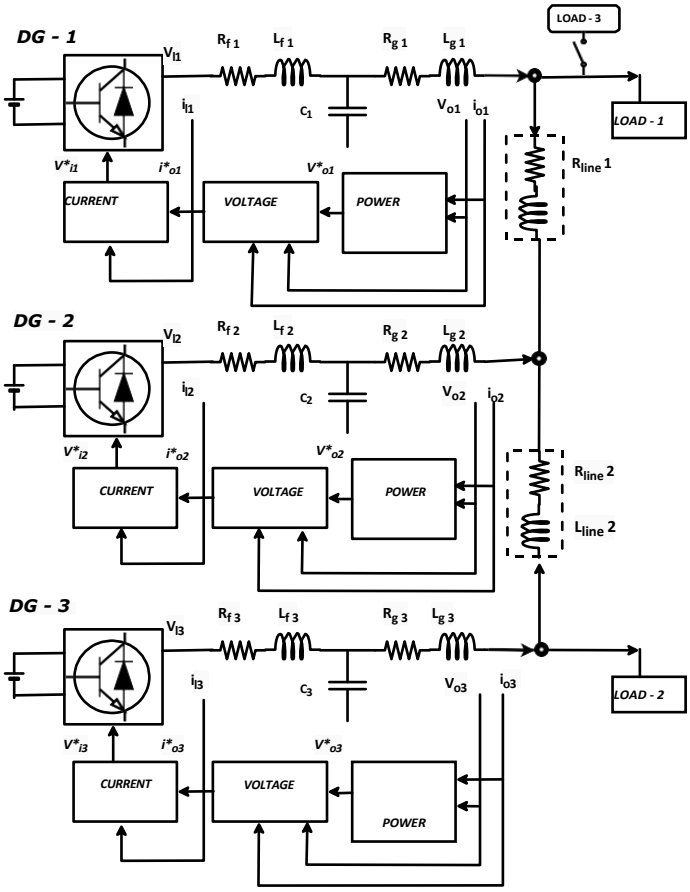


**Fig -7:** Circuit diagram of three VSI based standalone microgrid system.

## 5. RESULTS AND DISCUSSION

The proposed GCI system power rating is 10 kW with 3Φ-inductive load, as shown in Fig. 1, which is designed and tested in MATLAB/SIMULINK with m-files. The SIMULINK block diagram is given in Fig. 5. This paper validates the designed LCL filter for harmonic attenuation and verifies the stability conditions of the controller using the TYPHOON HIL emulator for real-time performance. The controller's design is primarily oriented towards enhancing tracking performance, especially in situations characterized by a less stable grid.

**TABLE - 5:** SELECTED PARAMETERS FOR THE EXPERIMENTAL SET-UP

| ***Parameters*** | ***Values*** |
|---|---|
| VSI Power rating | 10 kW |
| AC Voltage | 400 V |
| rated AC Current | 20 A |
| Input DC voltage ($V_{dc}$) | 850 V |
| Inverter-side inductance ($L_f$) | 2.53 mH |
| Grid-side inductance ($L_g$) | 2.53 mH |
| Filter Capacitance ($C_f$) | 10.03 $\mu$F |
| Damping resistor ($R_d$) | 1.588 $\Omega$ |
| 3$\Phi$ Inductive load | 1 kVA, 0.9 pf |
| Switching frequency ($f_{sw}$) | 20 kHz |
| AC frequency ($f_0$) | 50 Hz |
| Sampling Time ($T_s$) | 10 $\mu$s |
| Cut-off frequency ($\omega_c$) | 31.41 |
| $P-f$ droop gain ($m_p$) | 3.93e-4 |
| $Q-V$ droop gain ($n_q$) | 4.08e-3 |
| Resistance line - 1 ($R_{line}1$) | 0.23 $\Omega$ |
| Inductance line - 1 ($L_{line}1$) | 0.31 mH |
| Resistance line - 2 ($R_{line}2$) | 0.35 $\Omega$ |
| Inductance line - 2 ($L_{line}2$) | 1.85 mH |
| Load - 1 | 7 kVA, 0.9 pf |
| Load - 2 | 8 kVA, 0.9 pf |
| ***Parameters for Optimization algorithm*** | ***Values*** |
| Population size ($N_p$) | 50 |
| No. of iteration | 100 |
| Inertia constant ($w$) | 0.9 |
| Acceleration constant ($c_1 = c_2$) | 2 |
| Distribution index for crossover ($\eta_c$) | 20 |
| Distribution index for mutation ($\eta_m$) | 20 |
| Crossover Probability ($P_c$) | 0.8 |
| Mutation Probability ($P_m$) | 0.2 |
| Lower bound ($K_{P\ min}$, $K_{Imin}$) | 1.5, 1500 |
| Upper bound ($K_{pmax}$, $K_{Imax}$) | 3, 3000 |

The poles and zeros of the designed filter are in the left half of the s-plane, which represents the filter stability. By additional damping in the filter, the system stability is enhanced, shown in Fig 8 (a). As we increase the switching frequency, the filter becomes more effective at eliminating higher-order harmonics. To evaluate stability comprehensively, we have analyzed the gain and phase margins through the plant's transfer function and Bode plots, depicted in Fig. 8 (b). This analysis provides valuable insights into the filter's stability and its ability to suppress harmonics, essential for assessing its performance.

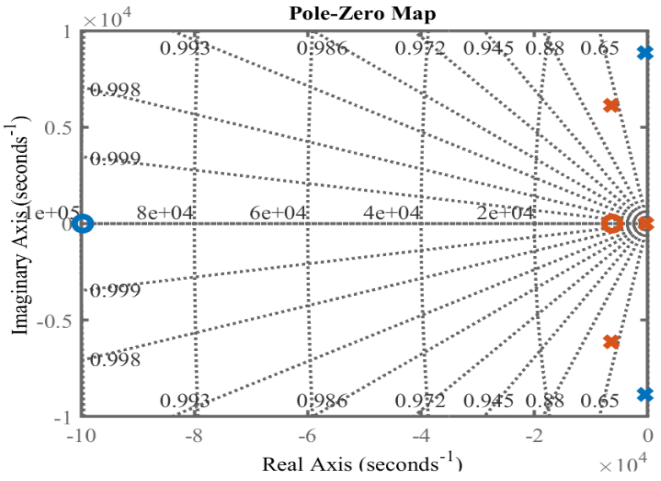


(a)

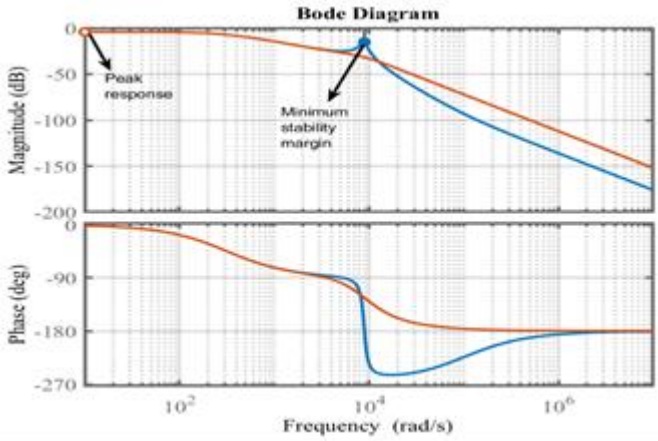


(b)

**Fig - 8:** Stability analysis**(a).** Pole and zeros of the closed loop system with (red) and without (blue) damping, **(b).** Bode plot of the plant transfer function with(red) and without(blue) damping

A higher switching frequency (refer to Table 5) is employed throughout the simulation. This higher frequency assists in the precise tracking of time-varying signals, compensating for dead time, and reducing current ripples in the output current.

The simulation parameters used for the system design are given in Table 5.

**Table - 6:** COMPARISON OF CONTROLLER GAIN VALUES AND STEADY-STATE RESPONSE WITH DIFFERENT CONTROLLER TUNING TECHNIQUES

| ***Items*** | ***Gain values*** ($K_p$, $K_I$) | $M_p$ | $T_{ss}$ ***(sec)*** |
|---|---|---|---|
| ***ZN method*** | 1.6821, 1587.06 | 12% | 100 |
| ***PSO*** | 2.5, 2944.6 | 19% | 89 |
| ***Real coded based GA*** | 2.2, 2316.3 | 15% | 95 |

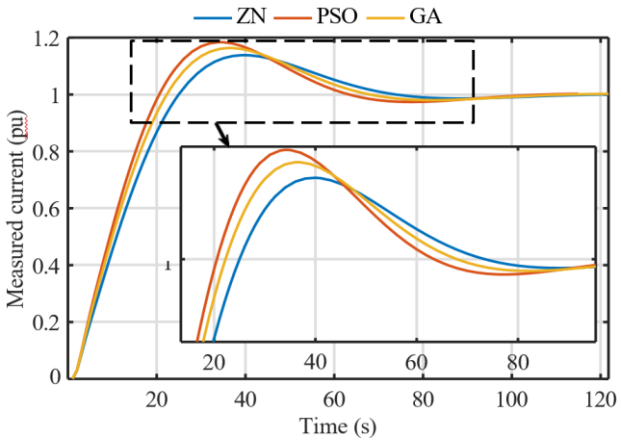


**Fig - 9:** PI controller gain response comparison with ZN, PSO and GA

The selected controller parameters are detailed in both Table 5 and Table 6. To initiate the optimization processes, the initial parameters for the PSO and GA are derived from the ZN method, which assists in establishing the upper and lower limits. In Fig. 9, a comparative analysis of the PI controller's settling time ($T_{ss}$) and maximum peak overshoot ($M_p$) is conducted across different tuning methods, including ZN, PSO, and GA, and the results are summarized in Table 6. Notably, GA outperforms the other methods by achieving $M_p$ value and $T_{ss}$ that aligns with the desired criteria. Consequently, the GA tuning method is selected for further experimental validation, as it meets all the specified criteria. The exploration into the controller's performance under weak grid conditions is prompted by the intermittent nature of renewable sources and variations in load-side impedance. In this context, the figures, specifically Fig. 10, 11, and 12, illustrate the dynamic response of the PI controller under various conditions during power regulation. These figures underscore the controller's efficacy in the nonlinear time domain, particularly when there are changes in current from 15A to 20A, demonstrating its dynamic response and its capability to control reactive power effectively.

The experiment aims to verify the obtained controller parameters from real-coded based GA, see Table 6, with the PI and PR controllers' performance for weak grid operating conditions based on $L_g$ variation and ($X/R$) variation, fault occurrence at the PCC and also tested for sudden load change in the standalone distributed network.

## 5.1 Parameter Variation Impact Analysis

### 5.1.1 Effects due to $L_g$ variations

In general, $L_g$ is kept lower than $L_f$ as suggested in many works of literature [36],[37]. Therefore, here the CCL performance is tested for the lower $L_g$ values to achieve the considered objective for the designed filter. The controller performance is responsible for controlling the active and reactive power supply to the utility, as shown in Fig. 10 (a)

and (b). The figure implies that the controller achieves the steady state within the standard time ($T_{ss}$ = 3 - 5 ms) and $M_p$ within 5% for the CCL. We find the $L_g$ variation for the transient condition in CCL, which could be responsible for the system's stability. The minimum $L_g$ value has the maximum $M_p$ and $T_{ss}$. The best controller tracking performance is obtained when $L_g$ is set to 2.53 mH, the $M_p$ and $T_{ss}$ are within the desired criteria, see in Fig. 10 (a). At this value, the inductance ratio ($a_L$) would be one, and the capacitor requires minimum energy storage, which also fulfills our filter design objective. From the above demonstration it is clear that as the controller performs worse as the $L_g$ value decreases, so it is important to maintain the grid impedance according to the connection requirements. In weak grid scenarios, it is better to consider equalizing the value of $L_f$ to reduce harmonics and current distortion at the load side.

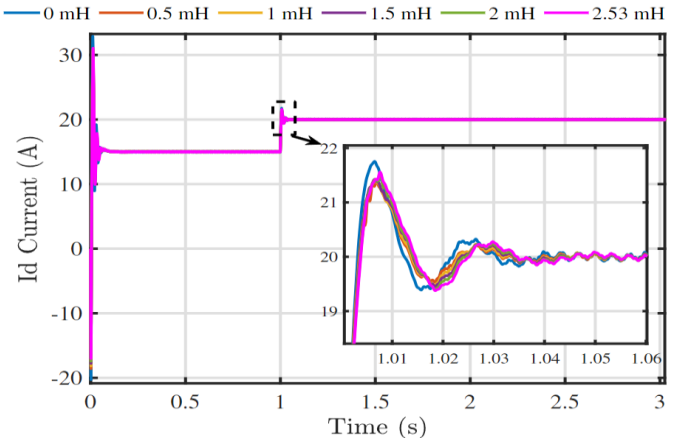


(a)

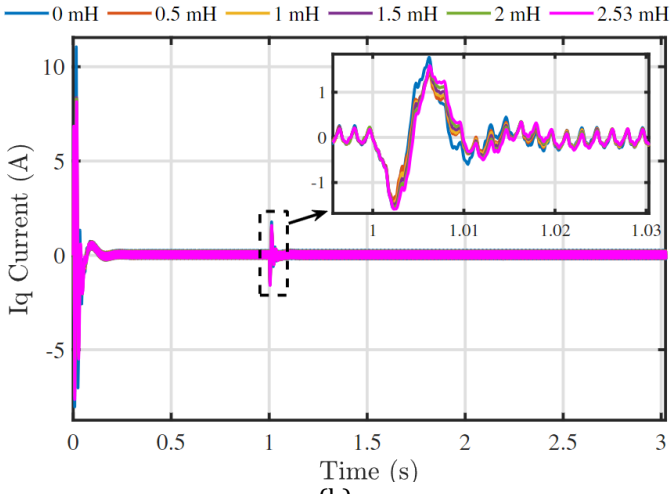


(b)

**Fig - 10:** (a). Comparison of $I_d$ current with $L_g$ variation, (b). Comparison of $I_q$ current with $L_g$ variation.

### 5.1.2 Effect on (X/R) variation

To study dynamic conditions, two types of disturbances are considered; a sudden change in power demand and a change in the line impedance. In a low voltage distribution network, the lower line impedance at the grid side, in case of sudden load changes, creates a severe problem that affects the controller performance and overall system efficiency (especially lower SCR value systems due to over-current). In Fig. 11 (a) and (b), the current is stepped up at 0.5 seconds to increase the power supply. The weak grid characteristics are defined as, SCR < 3 and (X/R) < 5 [11]. Where The SCR specifies the maximum amount of power that the power system can handle without compromising power quality at the PCC. As shown in Fig. 11 (a), the controller is quite robust to avoid the instability condition in the system and track the reference value with minimum oscillations. The best controller tracking performance with minimum ripple current (based on $T_{ss}$, $M_p$) is achieved when the (X/R) is equal to 2.5, which is within weak grid condition at the grid-side.

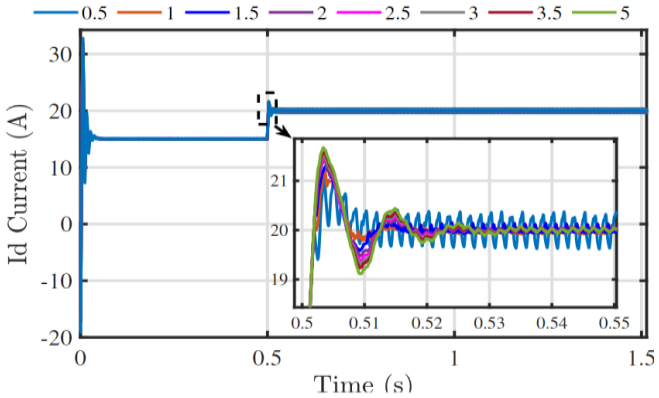


(a)

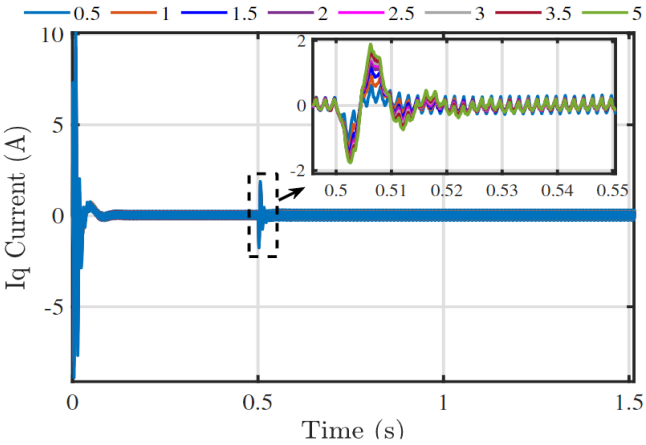


(b)

**Fig - 11:** (a). Comparison of $I_d$ current with (X/R) variation, (b). Comparison of $I_q$ current with (X/R) variation.

### 5.1.3 Effect of fault occurrence at PCC

Generally, a three-phase fault is considered for the controller performance and the system withstands capacity for the short circuit current analysis during transient conditions. Because the maximum fault current occurs in 3-phase fault.

When any fault occurs, the protection relay operating time is about 0.22 seconds [11]. The Critical Clearing Time (CCT) is a typical criterion for evaluating the transient stability limits. As we can see in Fig. 12, the fault is cleared within CCT, and the current signal is back on the track set by the controller. The controller limits the fault current during the fault condition and does not allow it to exceed the desired value. It shows the robustness of the controller and fault ride-through capability for lower strength systems to recover the voltage stability after the fault.

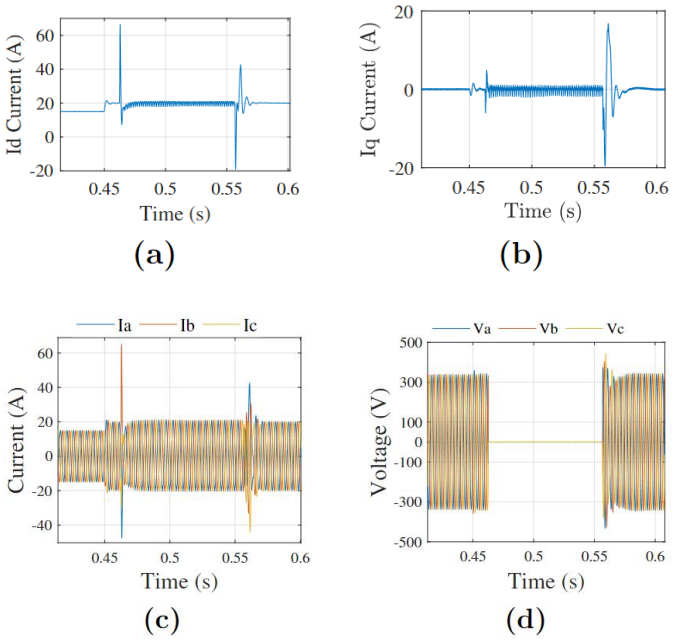


**Fig -12:** (a). $I_d$ current, (b). $I_q$ current, (c). VSI output 3ϕ - current during the fault condition, (d). Output 3ϕ - voltage during the fault condition.

### 5.1.4 THD Analysis

PI controller operates on a fixed frequency of the system, so its output could be unstable under weak grid conditions. But the PR controller has cut-off frequency bandwidth ($\omega_c$) around the system frequency, as discussed earlier in the current controller structure. For this experiment, the frequency variation is considered ±2Hz. The parameters are determined similarly to the PI controller to obtain the required closed-loop response from the PR controller. The cut-off frequency bandwidth can be extended by tuning the $\omega_c$. The higher value of $\omega_c$ is responsible for the increase in peak magnitude at the system frequency, which corresponds to a higher gain value and better current ripple attenuation. The lower value of $\omega_c$ corresponds to wider bandwidth at the system frequency [47]. The comparison for THD analysis by using PI and PR controller is shown in Fig. 13. The output current THD levels are below 3% as per requirements for the weak grid applications, which shows the quality of the output current.

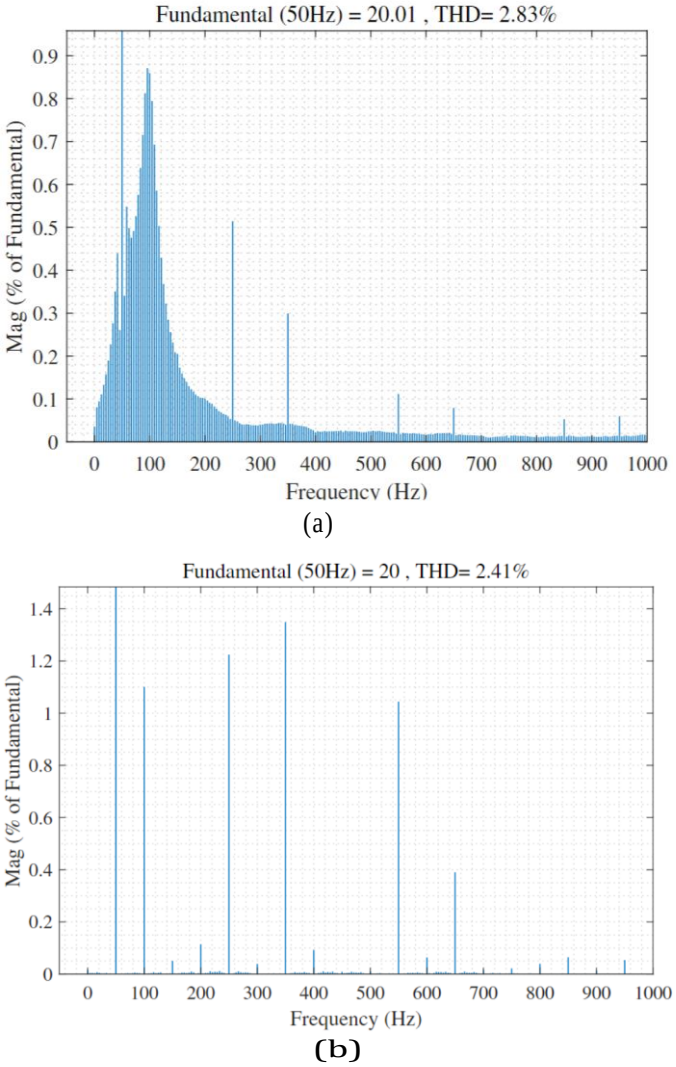


**Fig - 13**: THD analysis of VSI output current(a).for PI controller, (b). for PR controller.

### 5.1.5 Standalone Mode Controller Performance Analysis

In Fig. 7, the designed three VSIs (10kVA each) are connected to a distributed network in standalone mode for testing the stability and reliability performance. The eigenvalue spectrum of the consider network in Fig. 14 demonstrates the effectiveness of the designed controller system. The negative eigenvalues indicate that the system remains stable during standalone operation. The different cluster positions show the different modes in the microgrid system, such as distribution line, filter, power, voltage, and current controller state variables. Fig. 15 demonstrates the effectiveness of the controller tracking performance when there is a sudden 20% increase in load-1 at DG-1. The small load variation at a particular DG in the network, while here the load increase occurs at 0.5 seconds, leading to changes in active power sharing and consequently affecting the VSI frequency shown in the figure. However, active power oscillations may occur between parallel inverters during the

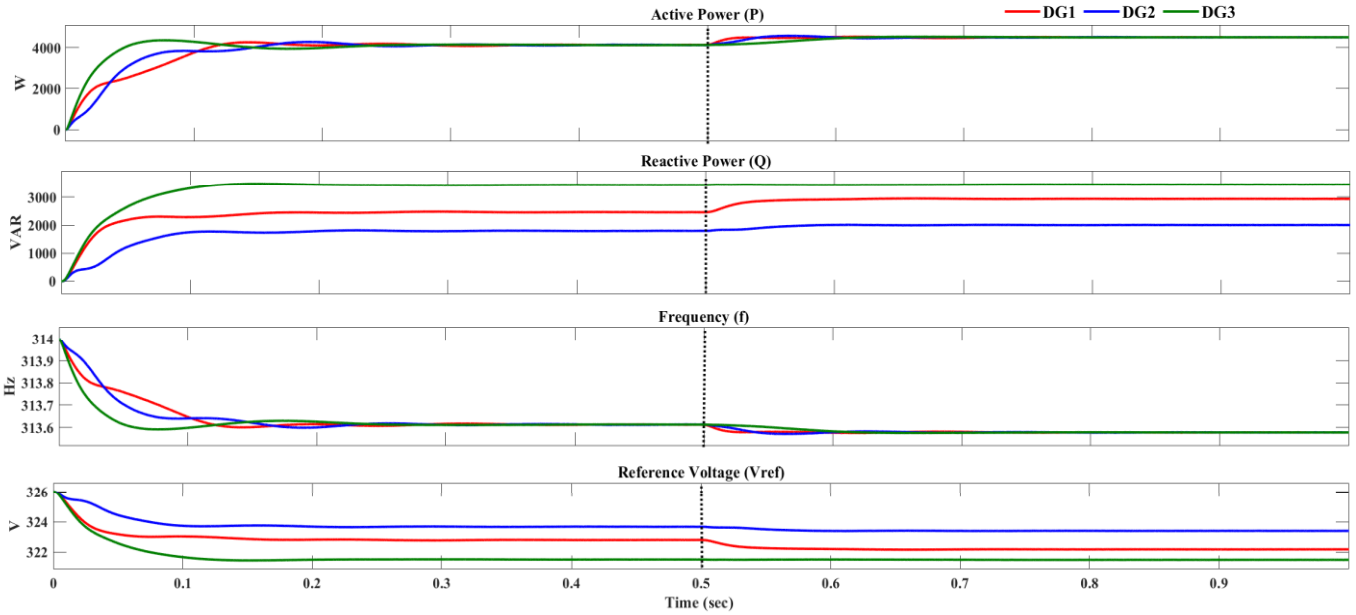


**Fig - 15:** Stability analysis of the three VSI standalone system when sudden load increased at 0.5 sec.

load fluctuations, but here the power flow is smooth without using any external damping techniques.

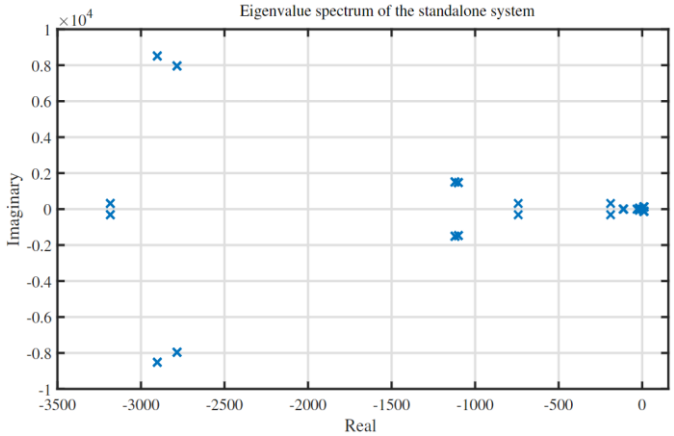


**Fig - 14:** Eigenvalue spectrum of three VSI in standalone mode

### 5.1.6 Controller Performance Validation

The plant function, considering all aspects outlined in section III, and tested it in MATLAB/SIMULINK. This testing helps us select accurate parameters in line with standard requirements [4], [9]. The controller gain values have been diligently calculated using three distinct methods to optimize controller performance during operation. These optimization algorithms have been implemented in custom m-files. The effectiveness of the controller loop optimization has been rigorously tested and verified using the Typhoon real-time emulator model-604, which provides an impressive 20-nsec sampling resolution. In Fig. 16, the schematic editor is used for VSI modeling purposes, which is compiled with the real-time hardware emulator set-up, and the SCADA (Supervisory Control and Data Acquisition) panel is used for monitoring and visualization of the output results.

The Typhoon set-up is connected through the Ethernet connection mode to the desktop system. The validation on Hardware-In-Loop implementation is completely reliable for the coordinated power feeding to the utility from different power generation sources through the connected power converter.

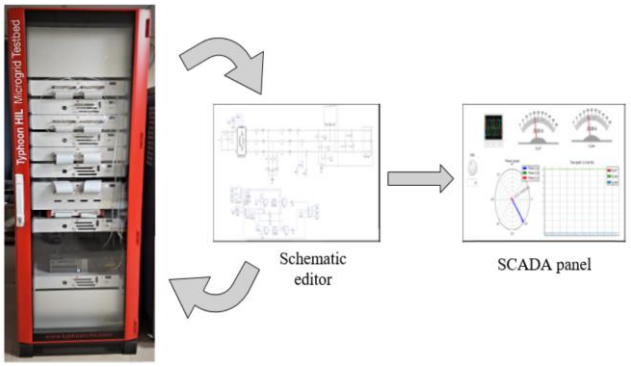


**Fig - 16:** HIL set-up :- Typhoon-Hil emulator 604 set-up in real-time mode.

### 5.1.7 Discussion

According to the findings in [9], the parameter optimization has yielded satisfactory results, as the THD level of the VSI output current remains consistently below 3%. In direct comparison to the results presented in [19], it is evident that the filter and controller parameters, as well as the resulting THD levels, are improved and better than the given results in the mentioned paper for the same inverter rating. Moreover, weak grid stability issues discussed in references such as [14] and [15] have been successfully addressed through the application of universal control modeling and various operating conditions tailored to weak grid scenarios. To mitigate the impact of grid- side impedance variations on

CCL, this study has systematically tested different controller tuning methods, meticulously documented in Table 6. The stability of the impedance variation-based controller performance is demonstrated in Fig. 10 and 11. The study's rigor extends to testing the VSI's performance during a three-phase fault occurrence at the PCC, as illustrated in Fig. 12. Furthermore, the VSI's performance was assessed in a standalone distributed network subjected to sudden load changes, revealing its robust controller tracking capabilities in parallel operation, which is vividly depicted in Fig. 15. The results collectively demonstrate that the designed VSI parameters are versatile and adept at handling a spectrum of scenarios, particularly in less stable conditions. The Comprehensive CCL tracking performance underscores the VSI's reliability even in challenging real-time conditions.

## 6. CONCLUSION

In this paper the grid impedance-based stability is concerned and improve the inverter stability for lower-voltage distribution networks. The calculated filter and controller parameters show their best performance for weak grid conditions. The GA results are the best option for the controller considerations for controller performance. Finally, it investigates the designed system parameters for controller tracking performance. The variations in Lg and (X/R) shows the impact on controller performance during grid-side impedance variations. The controller tracking performance is satisfactory for weak grid impedance scenarios. The performance at fault occurrence and sudden load change conditions shows the robustness of the system. To improve the THD level in the output current of the VSI, a PR controller is implemented, which shows an improved THD level compared to a PI controller. For future work on GCIs with weak grid conditions, two promising avenues for exploration include frequency stability or rate of change of frequency (ROCOF) of the VSI for grid synchronization and reactive power sharing management at the PCC.

## REFERENCES

[1]. R. Panigrahi, S. K. Mishra, S. C. Srivastava, A. K. Srivastava, N. N. Schulz, Grid integration of small-scale photovoltaic systems in secondary distribution network—a review, IEEE Trans. Ind. Appl. 56 (3) (2020) 3178–3195.
[2]. H. H. Figueira, H. L. Hey, L. Schuch, C. Rech, L. Michels, Brazilian grid-connected photo- voltaic inverters standards: A comparison with IEC and IEEE, in: 2015 IEEE 24th International Symposium on Industrial Electronics (ISIE), IEEE, 2015, pp. 1104–1109.
[3]. Y.-K. Wu, J.-H. Lin, H.-J. Lin, Standards and guidelines for grid-connected photovoltaic generation systems: A review and comparison, IEEE Trans. Ind. Appl. 53 (4) (2017) 3205–3216.
[4]. IEEE Standard for Interconnecting Distributed Resources with Electric Power Systems, IEEE std. 1547, 2003.
[5]. S. IEC, et al., Photovoltaic systems characteristics of the utility interface, IEC Std 61 (2004) 727.
[6]. I. S. 929-2000, IEEE recommended practice for utility interface of photovoltaic systems (2000).
[7]. E. VDE Association for Electrical, I. Technologies, VDE-AR-N 4105: 2011-08 power genera- tion systems connected to the low voltage distribution network (2011).
[8]. C. P. U. Commission, et al., Rule 21 generating facility interconnections, California Public Utilities Commission: San Francisco, CA, USA (2014).
[9]. T. M. Blooming, D. J. Carnovale, Application of IEEE std 519-1992 harmonic limits, in: Conference Record of 2006 Annual Pulp and Paper Industry Technical Conference, IEEE, 2006, pp. 1–9.
[10]. P. Channegowda, V. John, Filter optimization for grid interactive voltage source inverters, IEEE Trans. Ind. Electron. 57 (12) (2010) 4106–4114.
[11]. G. Jayasinghe, B. Bahrani, Stability-enhancing measures for weak grids study, Australian Renewable Energy Agency, Milestone2 report (June, 2021).
[12]. H. Alenius, M. Berg, R. Luhtala, T. Roinila, Stability and performance analysis of grid- connected inverter based on online measurements of current controller loop, in: IECON 2019- 45th Annual Conference of the IEEE Industrial Electronics Society, Vol. 1, IEEE, 2019, pp. 2013–2019.
[13]. D. Pattabiraman, R. Lasseter, T. Jahns, Comparison of grid following and grid forming control for a high inverter penetration power system, in: 2018 IEEE Power & Energy Society General Meeting (PESGM), IEEE, 2018, pp. 1–5.
[14]. Q. Zhang, M. Mao, G. Ke, L. Zhou, B. Xie, Stability problems of PV inverter in weak grid: a review, IET Power Electron. 13 (11) (2020) 2165–2174.
[15]. Q. Peng, Q. Jiang, Y. Yang, T. Liu, H. Wang, F. Blaabjerg, On the stability of power electronics-dominated systems: Challenges and potential solutions, IEEE Trans. Ind. Appl. 55 (6) (2019) 7657–7670.
[16]. M. B. Sa¨ıd-Romdhane, M. W. Naouar, I. Slama-Belkhodja, E. Monmasson, Robust active damping methods for LCL filter-based grid-connected converters, IEEE Trans. Power Elec- tron. 32 (9) (2016) 6739–6750.
[17]. L. Moretti, L. Meraldi, A. Niccolai, G. Manzolini, S. Leva, An innovative tunable rule-based strategy for the predictive management of hybrid microgrids, Electronics 10 (10) (2021) 1162.
[18]. M. Prodanovic, T. C. Green, Control and filter design of three-phase inverters for high power quality grid connection, IEEE Trans. Power Electron. 18 (1) (2003) 373–380.
[19]. E. Isen, A. F. Bakan, Development of 10 kw three-phase grid connected inverter, automatika 57 (2) (2016) 319–328.
[20]. J. Rocabert, A. Luna, F. Blaabjerg, P. Rodriguez, Control of power converters in ac micro- grids, IEEE Trans. Power Electron. 27 (11) (2012) 4734–4749.
[21]. D. G. Holmes, T. A. Lipo, B. P. Mcgrath, W. Y. Kong, Optimized design of stationary frame three phase AC current regulators, IEEE Trans. Power Electron. 24 (11) (2009) 2417–2426.

[22]. A. Timbus, M. Liserre, R. Teodorescu, P. Rodriguez, F. Blaabjerg, Evaluation of current controllers for distributed power generation systems, IEEE Trans. Power Electron. 24 (3) (2009) 654–664.
[23]. J. C. Basilio, S. Matos, Design of PI and PID controllers with transient performance specifi- cation, IEEE Trans. Educ. 45 (4) (2002) 364–370.
[24]. D. E. Rivera, M. Morari, S. Skogestad, Internal model control: PID controller design, Ind. Eng. Chem. Process Des. Dev. 25 (1) (1986) 252–265.
[25]. M. Hassan, M. Abido, Optimal design of microgrids in autonomous and grid-connected modes using particle swarm optimization, IEEE Trans. Power Electron. 26 (3) (2010) 755–769.
[26]. J. Hu, J. Zhu, D. G. Dorrell, Model predictive control of grid-connected inverters for PV systems with flexible power regulation and switching frequency reduction, IEEE Trans. Ind. Appl. 51 (1) (2014) 587–594.
[27]. Y. Del Valle, G. K. Venayagamoorthy, S. Mohagheghi, J.-C. Hernandez, R. G. Harley, Particle swarm optimization: basic concepts, variants and applications in power systems, IEEE Trans. Evol. Comput. 12 (2) (2008) 171–195.
[28]. J. Kennedy, R. Eberhart, Particle swarm optimization, in: Proceedings of ICNN'95- international conference on neural networks, Vol. 4, IEEE, 1995, pp. 1942–1948.
[29]. A. E. A. Awouda, R. B. Mamat, Refine PID tuning rule using ITAE criteria, in: 2010 The 2nd International Conference on Computer and Automation Engineering (ICCAE), Vol. 5, IEEE, 2010, pp. 171–176.
[30]. A. Rodr´ıguez-Molina, E. Mezura-Montes, M. G. Villarreal-Cervantes, M. Aldape-P´erez, Multi- objective meta-heuristic optimization in intelligent control: A survey on the controller tuning problem, Appl. Soft Comput. 93 (2020) 106342.
[31]. C. R. Os´orio, L. C. Borin, G. G. Koch, V. F. Montagner, Optimization of robust PI controllers for grid-tied inverters, in: 2019 IEEE 15th Brazilian Power Electronics Conference and 5th IEEE Southern Power Electronics Conference (COBEP/SPEC), IEEE, 2019, pp. 1–6.
[32]. A. C. Oliveira, C. B. Jacobina, A. M. N. Lima, Improved dead-time compensation for sinusoidal PWM inverters operating at high switching frequencies, IEEE Trans. Ind. Electron. 54 (4) (2007) 2295–2304.
[33]. H. Temiz, O. Keysan, E. Demirok, Adaptive controller based on grid impedance estimation for stable operation of grid-connected inverters under weak grid conditions, IET Power Electron. 13 (13) (2020) 2692–2705.
[34]. I. W. Group, et al., IEEE guide for planning dc links terminating at ac locations having low short-circuit capacities, Institute of Electrical and Electronics Engineers, Inc.: New York, NY, USA (1997).
[35]. Z. Zou, Z. Wang, M. Cheng, Modeling, analysis, and design of multifunction grid-interfaced inverters with output LCL filter, IEEE Trans. Power Electron. 29 (7) (2013) 3830–3839.
[36]. Y. Han, M. Yang, H. Li, P. Yang, L. Xu, E. A. A. Coelho, J. M. Guerrero, Modeling and stability analysis of LCL-type grid-connected inverters: a comprehensive overview, IEEE Access 7 (2019) 114975–115001.
[37]. S. Bernet, S. Ponnaluri, R. Teichmann, Design and loss comparison of matrix converters, and voltage-source converters for modern AC drives, IEEE Trans. Ind. Electron. 49 (2) (2002) 304–314.
[38]. M. Liserre, F. Blaabjerg, S. Hansen, Design and control of an LCL-filter-based three-phase active rectifier, IEEE Trans. Ind. Appl. 41 (5) (2005) 1281–1291.
[39]. T. C. Wang, Z. Ye, G. Sinha, X. Yuan, Output filter design for a grid-interconnected three- phase inverter, in: IEEE 34th Annual Conference on Power Electronics Specialist, 2003. PESC'03., Vol. 2, IEEE, 2003, pp. 779–784.
[40]. K. Jalili, S. Bernet, Design of LCL- filters of active-front-end two-level voltage-source con- verters, IEEE Trans. Ind. Electron. 56 (5) (2009) 1674–1689.
[41]. J. He, Y. W. Li, Generalized closed-loop control schemes with embedded virtual impedances for voltage source converters with LC or LCL filters, IEEE Trans. Power Electron. 27 (4) (2011) 1850–1861.
[42]. N. Pogaku, M. Prodanovic, T. C. Green, Modeling, analysis and testing of autonomous operation of an inverter-based microgrid, IEEE Trans. Power Electron. 22 (2) (2007) 613–625.
[43]. IEEE standard for Harmonic Control in Power Systems, Transmission and Distribution Com- mittee, IEEE Power and Energy Society (May, 2022).
[44]. IEEE std. 519-2014, IEEE Recommended Practices and Requirements for Harmonic Control in Electrical Power Systems, IEEE, New York (March, 2014).
[45]. P. D. Doman´ski, Control Performance Assessment: Theoretical Analyses and Industrial Prac- tice, Vol. 245, Springer, 2020.
[46]. K. Deb, K. Sindhya, T. Okabe, Self-adaptive simulated binary crossover for real-parameter optimization, in: Proceedings of the 9th annual conference on genetic and evolutionary computation, 2007, pp. 1187–1194.
[47]. M. Parvez, M. F. M. Elias, N. Abd Rahim, F. Blaabjerg, D. Abbott, S. F. Al-Sarawi, Comparative study of discrete PI and PR controls for single-phase UPS inverter, IEEE Access 8 (2020) 45584–45595.
[48]. Singh, H. P. and Swami A.K., "A Review of Power Quality Improvements by using FACTS devices". In The International Journal of Engineering and Science (IJES). 2019 Vol. 8. pp 53-64. DOI: 10.9790/1813-0806015364.
[49]. Singh H. P., Som S., Sharma A., Bose S. and Swami A.K. "Seamless transition of inverters from islanding to grid-connected mode connected to weak grid". IEEE Industrial Electronics Society Annual Online Conference (ONCON). 2023. DOI: 10.1109/ONCON60463.2023.10431030.
[50]. Singh, H. P., Sharma A., Bose S. and Swami A.K. 2024. "State space modelling and seamless transition between Islanded and Grid-connected operation modes". International Conference on Intelligent and Innovative Technologies in Computing, Electrical and Electronics (IITCEE) IEEE. DOI: 10.1109/IITCEE59897.2024.10467393.

## BIOGRAPHIES

**Harendra Pal Singh** received his B.Tech degree in Electrical and Electronics Engineering from Uttarakhand Technical University , India. His M.Tech in Power System Engineering from Uttarakhand Technical University , India. Currently, he is perusing PhD in Electrical Engineering from GBPUA&T, College of Technology, Pantnagar, India. He worked with UI-ASSIST project at IIT Kanpur, as Research Associate. He also has industrial experience.

His research interest includes microgrids, distributed power generation, application of power electronics in power system fields, optimization applications.

**Anurag K. Swami** is working as a professor at College of Technology, Pantnagar, Uttarakhand. His area of specialization is control applications in renewable energy systems and controller designing applications in different areas.